Fast and Accurate Spherical Harmonic Transform for Spatio-Temporal Regular Grid Data

Joydeep Chowdhury, Zubair Khalid, and Marc G. Genton

***Abstract*—We propose a fast and accurate spherical harmonic transform (SHT) to facilitate harmonic analysis of current and forthcoming high-resolution datasets acquired on a regular grid, commonly encountered in a variety of applications including but not limited to, medical imaging, geophysics, and climate studies. In contrast to other methods that take the points on the sphere on a Gaussian grid (non-uniform) or a pre-defined uniform grid parameterized by the band-limit (spectral truncation) of the data, the proposed method computes the SHT of the data available on a grid formed by the arbitrary number of equiangular latitudes and longitudes. Since the number of temporal observations in the spatio-temporal data can be in the millions, we also propose a pre-computation for SHT that does not alter the asymptotic computational complexity but results in a significant reduction in the computation time. Our analysis of accuracy and computation time on both synthetic and real datasets validates the proposed developments. To demonstrate the utility of the proposed method, we implement the spatial isotropy test using the largest eigenvalue of the correlation matrix of harmonic coefficients as a test statistic and demonstrate the superior performance of the proposed method in comparison to least-squares for computing SHT.**

***Index Terms*—Harmonic analysis, spatiotemporal analysis, spherical harmonic transform, sampling, isotropy.**

I. Introduction

THE use of spherical harmonics (natural basis functions on the sphere) [2] for the analysis of spatio-temporal data offers substantial advantages in the applications, where the observations are inherently defined on the sphere. Examples include spherical array beamforming in acoustics and communications [3], scattering networks for anisotropic filtering [4], 3D shape classification [5], stochastic generation of climate data [6], and cortical parcellation in medical imaging [7]. To support harmonic analysis in these applications, we address the need to develop a fast spherical harmonic transform (SHT) method for accurately representing high-resolution (in both space and time) spatio-temporal data on a uniform spherical grid with an arbitrary number of latitudes and longitudes.

Manuscript received 9 May 2024; revised 23 June 2024; accepted 24 June 2024. Date of publication 1 July 2024; date of current version 17 July 2024. This work was supported by the King Abdullah University of Science and Technology (KAUST). The associate editor coordinating the review of this manuscript and approving it for publication was Dr. Lu Gan. *(Corresponding author: Zubair Khalid.)*

Joydeep Chowdhury and Marc G. Genton are with the Statistics Program, King Abdullah University of Science and Technology, 23955, Saudi Arabia (e-mail: joydeep.chowdhury@kaust.edu.sa; marc.genton@kaust.edu.sa).

Zubair Khalid is with the Statistics Program, King Abdullah University of Science and Technology, 23955, Saudi Arabia, and also with the School of Science and Engineering, Lahore University of Management Sciences, Lahore 54792, Pakistan (e-mail: zubair.khalid@lums.edu.pk).

Digital Object Identifier 10.1109/LSP.2024.3420953

Noting the significance of analyzing the data in the harmonic domain (e.g., the European Centre for Medium-Range Weather Forecasts (ECMWF) has relied on spectral domain methods for over 40 years), there has been extensive exploration into the fast and accurate computation of SHT [8], [9], [10], [11], [12], [13], [14]. Existing methods for SHT have been developed for both regular grids [1], [8], [9], [10], [12], [15] and arbitrary grids [13]. For the regular grid formed by the Cartesian product of latitudes and longitudes, the existing methods use FFT along the longitude to speed up the computation and employ either the quadrature rule [8], [9], [10] or the least-squares method [1], [15] for evaluating the integral along latitude involved in the computation of SHT. Although the least-squares method proposed in [15] requires half the number of samples needed by the quadrature-based method, in general, quadrature-based methods outperform the least-squares method in terms of both computational efficiency and accuracy.

In spatial and spatio-temporal data analysis, the assumption of isotropy is crucial, as many methods rely on it (see, e.g., [16], [17], [18]). Existing methods for testing isotropy often consider the data as recorded on an Euclidean grid rather than on a sphere, resulting in an inaccurate representation of the underlying process. Recently, [1] considered geospatial data as observations recorded on a sphere, and employed the harmonic domain representations to construct a test of isotropy. However, the test was based on using the least-squares method for obtaining the SHT, making it computationally inefficient.

While quadrature-based methods support the sampling theorem on the sphere, they have been developed for uniform or Gaussian grids parameterized by the band-limit and cannot be readily used for grids with an arbitrary number of equiangular latitudes and longitudes. In this work, we address this limitation and present fast and accurate computation of SHT of the high-resolution spatio-temporal datasets. The proposed transform is adaptable to handle data on a grid formed by an arbitrary number of equiangular latitudes and longitudes. We analyse the computational complexity and storage requirements in case the pre-computation of data-independent evaluations is carried out to significantly reduce computation time and enable the scalability of SHT of the spatio-temporal dataset with a large number of temporal observations. We also carry out tests on both synthetic and real datasets to validate the proposed method. We illustrate the use of the proposed SHT for testing the spatial isotropy to demonstrate the higher statistical power of the test than the one proposed in the literature primarily due to accurate computation.

1070-9908 © 2024 IEEE. Personal use is permitted, but republication/redistribution requires IEEE permission.
See https://www.ieee.org/publications/rights/index.html for more information.

Authorized licensed use limited to: KAUST. Downloaded on July 22,2024 at 18:19:53 UTC from IEEE Xplore. Restrictions apply.

II. Preliminaries

A. Regular Grid Data Representation on the Sphere

The data are modeled or collected on the sphere (denoted by $\mathbb{S}^2$) as a function of two angles, namely co-latitude $0 \le \theta \le \pi$ and longitude $0 \le \phi < 2\pi$. The data samples are often taken on an equiangular regular grid $\mathcal{S}_{N_\theta,N_\phi}$ of $N_\theta \times N_\phi$ points comprised of N_θ equiangular iso-latitude rings with N_ϕ equiangular points in each ring along longitude and has T observations. It is worth noting that the temporal dimension T typically far exceeds the spatial resolution characterized by N_θ or N_ϕ. For example, one variable of the fifth generation ECMWF atmospheric reanalysis of the global climate (ERA5) dataset has $T \approx 0.7$ million hourly observations each defined on the grid $\mathcal{S}_{N_\theta,N_\phi}$ with $N_\theta = 721$ and $N_\phi = 1440$.

B. Spherical Harmonic Transform (SHT)

Spherical harmonic functions (or spherical harmonics) serve as an orthonormal basis for data on the sphere and are defined for integer degree $\ell \ge 0$ and integer order $|m| \le \ell$ as [2]

$$S_{\ell,m}(\theta,\phi) = \sqrt{\frac{2\ell+1}{4\pi}\frac{(\ell-m)!}{(\ell+m)!}} P_{\ell,m}(\cos\theta) e^{\mathrm{i}m\phi}, \quad (1)$$

where $P_{\ell,m}(\cdot)$ denotes the associated Legendre polynomial of degree ℓ and order m. The representation of data f on the sphere in terms of spherical harmonics is given by

$$f(\theta,\phi) = \sum_{\ell=0}^{\infty} \sum_{m=-\ell}^{\ell} f_{\ell,m} S_{\ell,m}(\theta,\phi), \quad (2)$$

where $f_{\ell,m}$ represents the spherical harmonic coefficient of degree ℓ and order m and is determined by the following spherical harmonic transform (SHT)

$$f_{\ell,m} = \int_{\theta\in[0,\pi]} \int_{\phi\in[0,2\pi)} f(\theta,\phi)\overline{S_{\ell,m}(\theta,\phi)} \sin\theta \mathrm{d}\phi \mathrm{d}\theta, \quad (3)$$

where $\overline{(\cdot)}$ denotes the complex conjugate operation.

C. Problem Under Consideration – Computation of SHT

For the efficient and accurate computation of SHT of the data f that is band-limited at degree L, satisfying $f_{\ell,m} = 0$ for all $\ell \ge L$ and $|m| \le \ell$, we can leverage specialized grids such as a pre-defined equiangular grid [8], [10] or a Gauss-Legendre grid [9], [19]. These grids facilitate efficient computation employing the fast Fourier transform and quadrature rules. Since the number of points along both the latitude and longitude in these sampling grids is characterized by the band-limit L, the spherical harmonic transforms associated with these sampling grids cannot be *readily* used for the data defined on a regular grid $\mathcal{S}_{N_\theta,N_\phi}$. Instead, we can opt for alternative approaches to recover the spherical harmonic coefficients. One commonly used technique is employing the least-squares method (e.g., [1]) which is both computationally intensive and prone to inaccuracies in the computation of SHT.

III. Spherical Harmonic Transform for Regular Grid Data

A. SHT Formulation

We substitute (1) in (3) to reformulate SHT as

$$f_{\ell,m} = \int_{\theta\in[0,\pi]} G_m(\theta) S_{\ell,m}(\theta,0) \sin\theta \mathrm{d}\theta, \quad (4)$$

with $S_{\ell,m}(\theta,\phi) = S_{\ell,m}(\theta,0)e^{\mathrm{i}m\phi}$ and

$$G_m(\theta) = \int_{\phi\in[0,2\pi)} f(\theta,\phi) e^{-\mathrm{i}m\phi} \mathrm{d}\phi. \quad (5)$$

Noting the representation of f in (2) in terms of spherical harmonics and employing the orthonormality of complex exponentials, $G_m(\theta)$ can be represented as

$$G_m(\theta) = 2\pi \sum_{\ell=|m|}^{L-1} f_{\ell,m} S_{\ell,m}(\theta,0), \quad (6)$$

which can be used to represent the data in the form:

$$f(\theta,\phi) = \sum_{m=-(L-1)}^{L-1} G_m(\theta) e^{-\mathrm{i}m\phi}. \quad (7)$$

Here we have assumed that the data are band-limited at degree L. We present a relationship between the maximum possible band-limit L and the number of points on the grid in the next section.

Noting the relationship between Wigner-d function, denoted by $d^\ell_{m,n}(\theta)$ for degree ℓ and orders $|m|, |n| \le \ell$, and the spherical harmonic given by [2]: $S_{\ell,m}(\theta,0) = \sqrt{\frac{2\ell+1}{4\pi}} d^\ell_{m,0}(\theta)$, and the following expansion of Wigner-d function in terms of complex exponentials [2], [20]: $d^\ell_{m,0}(\theta) = \mathrm{i}^{-m} \sum_{m'=-\ell}^{\ell} d^\ell_{m',0}(\frac{\pi}{2})\, d^\ell_{m',m}(\frac{\pi}{2})\, e^{\mathrm{i}m'\theta}$, we can write (6) after interchanging the order of summation as

$$G_m(\theta) = \sum_{m'=-(L-1)}^{L-1} K_{m,m'}\, e^{\mathrm{i}m'\theta}, \quad (8)$$

where $K_{m,m'} = \mathrm{i}^{-m} \sum_{\ell=\max(|m'|,|m|)}^{L-1} \sqrt{(\pi)(2\ell+1)}\, f_{\ell,m} \times d^\ell_{m',0}(\frac{\pi}{2})\, d^\ell_{m',m}(\frac{\pi}{2})$. By substituting (8) in (4), we obtain

$$f_{\ell,m} = \sum_{m''=-(L-1)}^{L-1} Q_{\ell,m,m''} \sum_{m'=-(L-1)}^{L-1} K_{m,m'}\, I(m'+m''), \quad (9)$$

where

$$Q_{\ell,m,m''} = \mathrm{i}^{-m} \sqrt{\frac{2\ell+1}{4\pi}} d^\ell_{m'',0}\left(\frac{\pi}{2}\right)\, d^\ell_{m'',m}\left(\frac{\pi}{2}\right). \quad (10)$$

$I(q)$ is an integral of the form

$$I(q) = \int_{\theta\in[0,\pi]} e^{\mathrm{i}q\theta} \sin\theta \mathrm{d}\theta = \begin{cases} \delta_{|q|,1} \frac{\mathrm{i}q\pi}{2}, & q \text{ odd}, \\ \frac{2}{1-q^2}, & q \text{ even}, \end{cases} \quad (11)$$

where $\delta_{|q|,1}$ is a Kronecker delta function.

B. Fast Computation

Instead of evaluating the integrals along latitude and longitude in (4) and (5) respectively, our approach requires the computation of $G_m(\theta)$ for each grid point θ and $K_{m,m'}$ for all $|m|, |m'| < L$. Since the representation of the data in (7) indicates that $f(\cdot,\phi)$, with complex exponentials $\{e^{\mathrm{i}m\phi}\}$ as basis functions, is band-limited at L, $G_m(\theta)$ can be recovered accurately using FFT if $N_\phi \ge 2L-1$. We use (8) to recover $K_{m,m'}$ by employing inverse FFT provided $G_m(\theta)$ is given for the sufficient number of co-latitude points over the domain $[0, 2\pi)$. We have $G_m(\theta)$ over N_θ equiangular points over the domain $[0,\pi]$ with two samples at the poles ($\theta = 0, \pi$). Noting (6), we extend the domain of $G_m(\theta)$ to include the points along co-latitude in $(\pi, 2\pi)$ for $\theta \in (0,\pi)$ as

$$G_m(2\pi-\theta) = 2\pi \sum_{\ell=|m|}^{L-1} f_{\ell,m} S_{\ell,m}(\theta,\pi) = (-1)^m G_m(\theta),$$

where we have used $(-1)^m S_{\ell,m}(\theta,\pi) = S_{\ell,m}(\theta,0)$. Once we have $K_{m,m'}$, we use (9) for the computation of SHT.

Authorized licensed use limited to: KAUST. Downloaded on July 22,2024 at 18:19:53 UTC from IEEE Xplore. Restrictions apply.

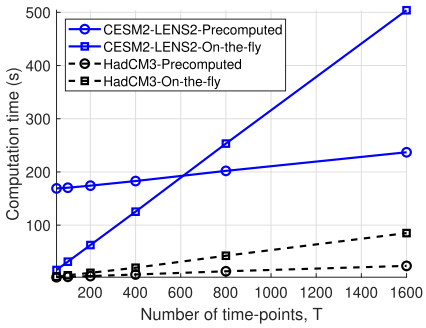

Fig. 1. Computation time taken by the proposed SHT applied to HadCM3 and CESM2-LENS2 datasets for different time points, T.

Remark 1: (On the choice of band-limit of the data taken on a regular grid $\mathcal{S}_{N_\theta,N_\phi}$). Our approach requires the accurate computation of $G_m(\theta)$ and $K_{m,m'}$ for all $|m|, |m'| < L$ from the data collected on $\mathcal{S}_{N_\theta,N_\phi}$ with N_ϕ points along longitude and $2N_\theta - 2$ points along extended co-latitude. Noting (6) and (8), $G_m(\theta)$ and $K_{m,m'}$ can be exactly computed if

$$L \leq \min\left(N_\theta - 1, \left\lfloor \frac{N_\phi + 1}{2} \right\rfloor\right). \tag{12}$$

C. Computation Complexity and Storage Requirements

We analyze the computational complexity and storage requirements in terms of the band-limit and the number of temporal observations (each defined on the sphere on a grid $\mathcal{S}_{N_\theta,N_\phi}$). For the fast computation of SHT, we propose to pre-compute the matrices or variables that are not dependent on the data so that they are not computed for each temporal observation. For the data sampled on the grid $\mathcal{S}_{N_\theta,N_\phi}$, $G_m(\theta)$ and $K_{m,m'}$ can be computed in $O(L^2 \log L)$ since both requires the use of FFT (either along ϕ or extended θ). Once we have $K_{m,m'}$ for all $|m|, |m'| < L$ for each observation, the inner summation in (9) can be computed with computational complexity $O(L^3)$ for all m and m''. After the evaluation of inner summation, the outer summation also takes $O(L^3)$ for each observation, resulting in overall complexity of $O(TL^3)$ for all temporal observations. Wigner-d functions for the fixed argument $\pi/2$ can be computed using the recursion relations [21]. Such computation takes $O(\ell^2)$ to compute $d^{\ell}_{m'',m}(\frac{\pi}{2})$ using $d^{\ell-1}_{m'',m}(\frac{\pi}{2})$ for all orders, and therefore takes $O(L^3)$ for all degrees and orders. The computation of $Q_{\ell,m,m'}$ as expressed in (10) takes $O(L^3)$. Since $Q_{\ell,m,m'}$ is independent of the data, we can pre-compute it for $\ell < L$, $|m| \leq \ell$, and $|m'| < L$, requiring $O(L^3)$ storage.

The pre-computation in our approach does not improve the asymptotic computation complexity of the SHT but brings about a substantial improvement in computation time. This is illustrated in Fig. 1, where we plot the computation time[1] taken by our proposed SHT method, both with and without pre-computation, applied to datasets from Hadley Centre Coupled Model version 3 (HadCM3) and Community Earth System Model version 2 Large Ensembles (CESM2-LENS2). The HadCM3 and CESM2-LENS2 observations are represented on the grid $\mathcal{S}_{N_\theta,N_\phi}$ with dimensions $N_\theta = 73$, $N_\phi = 96$ and $N_\theta = 192$, $N_\phi = 288$, respectively. The plots not only reaffirm the theoretical complexity of our SHT method but also underscore the substantial time savings offered by our approach, particularly evident for larger values of T for which the pre-computation surpasses the speed of on-the-fly computations.

[1]We recorded the computation times for different time points using Matlab version R2023b running on a Linux server equipped with Intel(R) Xeon(R) Gold 6230R CPU 2.10 GHz processor and 256 GB RAM.

TABLE I
ESTIMATED SIZES OF THE SHT-BASED TEST AT 5% NOMINAL LEVEL, BASED ON 1000 INDEPENDENT REPLICATIONS

$\mathcal{S}_{20,50}$			$\mathcal{S}_{73,96}$			$\mathcal{S}_{100,200}$		
ℓ	$C_{\ell 2}$	$C_{\ell 3}$	ℓ	$C_{\ell 2}$	$C_{\ell 3}$	ℓ	$C_{\ell 2}$	$C_{\ell 3}$
3	0.051	0.053	5	0.056	0.052	5	0.041	0.046
4	0.059	0.06	10	0.048	0.045	10	0.044	0.049
5	0.057	0.06	15	0.05	0.056	15	0.056	0.056
8		0.058	20	0.054	0.059	25	0.059	0.059
10		0.055	24	0.056	0.054	35	0.058	0.061
15		0.056	27	0.049	0.056	45	0.052	0.049
			29	0.059	0.057	55	0.058	0.042
			35		0.049	65	0.056	0.059
			40		0.045	70	0.049	0.061
			45		0.059	74	0.04	0.059

D. Accuracy Validation

To validate the proposed transform's accuracy, we use HadCM3 project grid $\mathcal{S}_{N_\theta,N_\phi}$ with $N_\theta = 73$ and $N_\phi = 96$. Noting (12), we can compute SHT exactly if the data have a maximum band-limit of 48. We generate $T = 100$ realizations of synthetic data on the grid for different band-limits $1 \leq L \leq 48$ by generating the coefficients $f_{\ell,m}$ of the data with real and imaginary parts uniformly distributed in $(-1, 1)$, normalizing the coefficients such that $\sum_{\ell=0}^{L-1} \sum_{m=-\ell}^{\ell} |f_{\ell,m}|^2 = 1$ and then synthesizing the data on $\mathcal{S}_{N_\theta,N_\phi}$ using (2). We apply our proposed SHT and compute the mean-squared error (MSE) between the original and computed coefficients. The resulting MSE falls within the range of 10^{-15} to 10^{-16} for all band-limits, indicating that the proposed method computes SHT with errors consistently within the range of numerical precision. We also analyze the accuracy using daily observations of the HadCM3 project for the years 2031-2035. We compute the SHT for each observation and use the spherical harmonic coefficients to reconstruct the data on the $\mathcal{S}_{N_\theta,N_\phi}$ using (2). Since the underlying process is *not* band-limited, the MSE between the reconstructed data and the original data is in the range of 10^{-5}, indicating the numerical accuracy of the SHT.

IV. APPLICATION: TEST OF ISOTROPY

We demonstrate the significantly higher statistical power achieved through the use of our method in the testing procedure suggested in [1] for testing spatial isotropy.

A. Isotropy in Spatial and Harmonic Domains

If the random field $Y_t(\theta, \phi)$ on the sphere for time $t = 1, 2, \ldots, T$ is assumed to be a Gaussian process, the process is isotropic if the mean function $\mathrm{E}[Y_t] = \mu$ is constant (or zero without loss of generality) and the covariance function $\mathrm{cov}(Y_t(\theta_1, \phi_1), Y_t(\theta_2, \phi_2))$, denoted by K, depends on the great-circle distance between the points $\hat{\boldsymbol{x}}$ and $\hat{\boldsymbol{y}}$ on the sphere characterized by (θ_1, ϕ_1) and (θ_2, ϕ_2) respectively [1], i.e.,

$$\mathrm{cov}(Y_t(\theta_1, \phi_1), Y_t(\theta_2, \phi_2)) = K(\hat{\boldsymbol{x}} \cdot \hat{\boldsymbol{y}}), \tag{13}$$

where $(\cdot)$ indicates the dot product. Noting the harmonic representation of $Y_t(\theta, \phi)$ given by $w_{\ell,m,t}$, the characterization in (13)

Authorized licensed use limited to: KAUST. Downloaded on July 22,2024 at 18:19:53 UTC from IEEE Xplore. Restrictions apply.

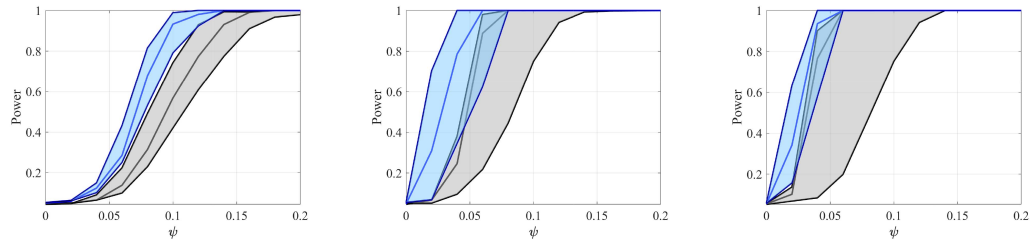

(a) $\mathcal{S}_{20,50}$ (b) $\mathcal{S}_{73,96}$ (c) $\mathcal{S}_{100,200}$

Fig. 2. Estimated powers for the isotropy testing procedure (blue) compared to the procedure in [1] (grey) for the axially symmetric process.

makes the harmonic coefficients uncorrelated, that is,

$$\mathrm{E}[y_{\ell,m,t}\,\overline{y_{\ell',m',t}}] = \delta_{\ell,\ell'}\,\delta_{m,m'}\,C_\ell, \tag{14}$$

where C_ℓ is the power spectrum of the process for degree ℓ.

B. Isotropy Test

The simple characterization of isotropy of a Gaussian process in the harmonic domain leads to a procedure for testing isotropy developed in [1] based on the correlation matrix of the spherical harmonic coefficients $y_{l,m,t}$ estimated using a least-squares procedure from the samples taken on the grid $\mathcal{S}_{N_\theta,N_\phi}$. Let $\mathbf{R}$ denote the correlation matrix of the vector $\mathbf{Y}_t$ containing all the coefficients $\{y_{l,m,t}\}$ for fixed t. Then, the testing of isotropy is equivalent to testing

$$\mathrm{H}_0 : \mathbf{R} = \mathrm{I} \quad \text{vs} \quad \mathrm{H}_1 : \mathbf{R} \neq \mathrm{I},$$

where I denotes the identity matrix. When the null hypothesis H_0 is true, all the eigenvalues of the correlation matrix $\mathbf{R}$ are equal, each being 1. On the other hand, if H_0 is false, the largest eigenvalue deviates from 1. Based on this observation, a test for H_0 is implemented by [1] using the largest eigenvalue of the estimated correlation matrix of $\mathbf{Y}_t$. The null distribution of the test statistic is obtained by [1] using the fact that under the null hypothesis, the largest eigenvalue of the estimated correlation matrix of $\mathbf{Y}_t$ follows the Tracy-Widom law of order 1, which stems from results derived in [22].

C. Illustration Using Simulated Data

We demonstrate here the estimated sizes and powers of the isotropy test conducted using the proposed method in comparison to the least-squares method proposed in [1]. We consider the simulation setup similar to [1] (see Section 4). We denote the quantities $C_{\ell 2} = \sigma^2/(\alpha^2+\ell^2)$ and $C_{\ell 3} = \sigma^2/(\alpha^2+\ell^2)^{3/2}$, where α^2 and σ^2 are real-valued parameters and ℓ is another parameter taking values in the set of natural numbers. We generate independent Gaussian random variables

$$a_{00} \sim N(0, 1.5), \quad \mathrm{Re}(a_{\ell mt}), \mathrm{Im}(a_{\ell mt}) \sim N(0, C_\ell/2),$$

where $\ell = 1, \ldots, \ell_{\mathrm{sim}} = 150$ and $t = 1, 2, \ldots, 360$. We consider three grids: $\mathcal{S}_{20,50}$, $\mathcal{S}_{73,96}$, and $\mathcal{S}_{100,200}$, and the choices of ℓ_{reg} and ℓ_{corr} are the same as considered in Table 1 in [1]. The estimated sizes of the proposed procedure are computed based on 1000 independent replications and are presented in Table I, which indicates that the testing procedure is properly sized. Next, the estimated powers of the proposed procedure are compared with the test of isotropy developed in [1] for an axially symmetric process. Here the random variables $a_{\ell mt}$ follow the relation $a_{\ell mt} = \sqrt{C_{\ell 2}}(B_{\ell mt} + e_{\ell mt})$, with $B_{\ell mt}$ being a complex Gaussian random variable with variance 0.5 and $\mathrm{corr}(B_{\ell mt}, B_{\ell' m' t}) = \psi I(\ell \neq \ell', m = m')$, and $0 \leq \psi \leq 1$. $e_{\ell mt}$ is also a complex Gaussian random variable with variance 0.5 but independent of $B_{\ell mt}$ and independent of other $e_{\ell mt}$ for different values of the tuple (ℓ, m, t). For the same grid sizes, the power of the proposed procedure is estimated for 1000 independent replications. To reduce clutter, the different curves for the different values of ℓ are represented by the band formed by them in Fig. 2 with the leftmost curve for the largest value of ℓ, clearly indicating significantly higher statistical power for the use of our method in testing isotropy.

D. Illustration Using Real Data

We consider HadCM3 data analyzed in [1]. The goal of this analysis is to compare the p-values of our proposed procedure with the p-values presented in [1]. We consider the same three models M_1, M_2 and M_3 considered in Section 5 in [1]. The three models are progressively complex and aim to capture more of the anisotropic component present in the sample. Model M_1 only separates a spatially varying mean from the data, while model M_2 captures a seasonally varying temporal component in addition to the spatially varying mean, and finally model M_3 assumes a spatially varying variance in addition to the components captured in model M_2. We obtain all p-values equal to zero with the test statistic values of 945, 710 and 322 as opposed to 958, 716 and 328 obtained in [1].

V. Conclusion

We have proposed efficient and accurate SHT for high-resolution global spatio-temporal datasets. Our method is adaptable for grids commonly encountered in different applications, formed by an arbitrary number of equiangular latitudes and longitudes. The proposed pre-computation significantly reduces the computation. We have validated the numerical correctness of the proposed method on both synthetic and real datasets and demonstrated its superior statistical power in assessing spatial isotropy. Since the proposed formulation is completely parallelizable, it has a potential for implementation on supercomputers with computational complexity linear with the band-limit in the spherical harmonic domain - a consideration to be explored in detail in future work.

Acknowledgment

The authors would like to acknowledge Prof. I. Sahoo for providing the code related to the work presented in [1].

Authorized licensed use limited to: KAUST. Downloaded on July 22,2024 at 18:19:53 UTC from IEEE Xplore. Restrictions apply.

REFERENCES

[1] I. Sahoo, J. Guinness, and B. J. Reich, "A test for isotropy on a sphere using spherical harmonic functions," *Statistica Sinica*, vol. 29, no. 3, pp. 1253–1276, 2019.

[2] R. A. Kennedy and P. Sadeghi, *Hilbert Space Methods in Signal Processing*. Cambridge, U.K.: Cambridge Univ. Press, Mar. 2013.

[3] S. K. Yadav and N. V. George, "Sparse distortionless modal beamforming for spherical microphone arrays," *IEEE Signal Process. Lett.*, vol. 29, pp. 2068–2072, 2022.

[4] Y. Xiong, W. Dai, W. Fei, S. Li, and H. Xiong, "Anisotropic spherical scattering networks via directional spin wavelet," *IEEE Trans. Signal Process.*, vol. 71, pp. 2981–2996, 2023.

[5] A. Mukhaimar, R. Tennakoon, C. Y. Lai, R. Hoseinnezhad, and A. Bab-Hadiashar, "Robust object classification approach using spherical harmonics," *IEEE Access*, vol. 10, pp. 21541–21553, 2022.

[6] Y. Song, Z. Khalid, and M. G. Genton, "Efficient stochastic generators with spherical harmonic transformation for high-resolution global climate simulations from CESM2-LENS2," *J. Amer. Statist. Assoc.*, 2023, doi: 10.1080/01621459.2024.2360666.

[7] S. Ha and I. Lyu, "SPHARM-Net: Spherical harmonics-based convolution for cortical parcellation," *IEEE Trans. Med. Imag.*, vol. 41, no. 10, pp. 2739–2751, Oct. 2022.

[8] J. R. Driscoll and D. M. Healy Jr., "Computing Fourier transforms and convolutions on the 2-sphere," *Adv. Appl. Math.*, vol. 15, no. 2, pp. 202–250, Jun. 1994.

[9] A. Doroshkevich et al., "Gauss–Legendre sky pixelization (GLESP) for CMB maps," *Int. J. Modern Phys. D*, vol. 14, no. 02, pp. 275–290, 2005.

[10] J. D. McEwen and Y. Wiaux, "A novel sampling theorem on the sphere," *IEEE Trans. Signal Process.*, vol. 59, no. 12, pp. 5876–5887, Dec. 2011.

[11] Z. Khalid, R. A. Kennedy, and J. D. McEwen, "An optimal-dimensionality sampling scheme on the sphere with fast spherical harmonic transforms," *IEEE Trans. Signal Process.*, vol. 62, no. 17, pp. 4597–4610, Sep. 2014.

[12] N. P. Wedi, M. Hamrud, and G. Mozdzynski, "A fast spherical harmonics transform for global NWP and climate models," *Monthly Weather Rev.*, vol. 141, no. 10, pp. 3450–3461, 2013.

[13] N. R. Cavanaugh, T. A. O'Brien, W. D. Collins, and W. C. Skamarock, "Spherical harmonic spectral estimation on arbitrary grids," *Monthly Weather Rev.*, vol. 145, no. 8, pp. 3355–3363, 2017.

[14] M. S. A. Khan, S. Nadeem, and Z. Khalid, "Sampling order-limited signals on the sphere," in *Proc. IEEE Int. Conf. Acoust. Speech Signal Process.*, 2023, pp. 1–5.

[15] J. Blais, "Discrete spherical harmonic transforms for equiangular grids of spatial and spectral data," *J. Geodetic Sci.*, vol. 1, no. 1, pp. 9–16, 2011.

[16] M. G. Genton, "Classes of kernels for machine learning: A statistics perspective," *J. Mach. Learn. Res.*, vol. 2, pp. 299–312, Dec. 2001.

[17] E. Porcu, J. Mateu, A. Zini, and R. Pini, "Modelling spatio-temporal data: A new variogram and covariance structure proposal," *Statist. Probability Lett.*, vol. 77, no. 1, pp. 83–89, 2007.

[18] J. Jeong, M. Jun, and M. G. Genton, "Spherical process models for global spatial statistics," *Stat. Sci.*, vol. 32, no. 4, pp. 501–513, 2017.

[19] Z. Khalid, S. Durrani, R. A. Kennedy, Y. Wiaux, and J. D. McEwen, "Gauss–Legendre sampling on the rotation group," *IEEE Signal Process. Lett.*, vol. 23, no. 2, pp. 207–211, Feb. 2016.

[20] T. Risbo, "Fourier transform summation of legendre series and d-functions," *J. Geodesy*, vol. 70, no. 7, pp. 383–396, Jul. 1996.

[21] S. Trapani and J. Navaza, "Calculation of spherical harmonics and wigner d functions by FFT. Applications to fast rotational matching in molecular replacement and implementation into AMoRe," *Acta Crystallogr. A*, vol. 62, no. 4, pp. 262–269, Jul. 2006.

[22] I. M. Johnstone, "On the distribution of the largest eigenvalue in principal components analysis," *Ann. Statist.*, vol. 29, no. 2, pp. 295–327, 2001.

Authorized licensed use limited to: KAUST. Downloaded on July 22,2024 at 18:19:53 UTC from IEEE Xplore. Restrictions apply.